Modification of Chitosan using Fe_3O_4 and Glucose and Its Application for Phenol Removal

Widya Twiny Rizki[1,2*], Siti Marwah Lestari[1], Vindi Annisa Rahmah[1], and Rd Rahmat Dauli[3]

[1]*Department of Pharmacy, Faculty of Health Sciences, Adiwangsa Jambi University, Jl. Sersan Muslim, RT 24, Thehok, Jambi 36138, Indonesia*

[2]*Department of Chemistry, Faculty of Science and Technology, Universitas Jambi, Jl. Raya Jambi Km. 15, Muara Bulian, Mendalo Indah, Jambi 36361, Indonesia*

[3]*Department of Information System, Faculty of Engineering and Computer Science, Adiwangsa Jambi University, Jl. Sersan Muslim RT 24, Thehok, Jambi 36138, Indonesia*

* ***Corresponding author:***

email: widyatwinirizki@gmail.com

Received: December 27, 2024
Accepted: April 12, 2025

DOI: 10.22146/ijc.103140

Abstract: *In this study, chitosan was modified with Fe_3O_4 and glucose to enhance its capacity and effectiveness in adsorbing phenol from organic waste. XRD analysis revealed distinct differences between unmodified chitosan and the Fe_3O_4/glucose-modified version, with the resulting nanocomposite showing a particle size of 17.21 nm. FTIR spectra exhibited new, sharper peaks at 531 and 544 cm^{-1}, indicating interactions between chitosan and Fe_3O_4 via the nitrogen atom in the NH_2 group. VSM characterization showed a saturation magnetization of 63.4 emu/g, confirming that the chitosan/Fe_3O_4/glucose nanocomposite is superparamagnetic. SEM analysis revealed an uneven, porous surface, while the morphology displayed dark Fe_3O_4 spots dispersed across a lighter chitosan matrix. The optimal adsorption condition was achieved at a contact time of 60 min, with an adsorption efficiency of 16.46%. In addition to reducing phenol content in wastewater, the modified nanocomposite also exhibited antibacterial activity against* Staphylococcus aureus *and* Escherichia coli. *This multifunctional material offers a promising solution for wastewater treatment, targeting both organic pollutants and pathogenic bacteria to help address water pollution challenges.*

Keywords: *chitosan; adsorption; phenol; glucose; antibacterial*

■ INTRODUCTION

Water pollution caused by organic waste is a serious environmental issue that has attracted serious attention over the past few decades. Organic pollutants such as phenol are particularly concerning due to their potential to cause severe damage to aquatic ecosystems [1]. Phenol waste originates from various industrial activities, including petroleum refining, petrochemicals production, coal conversion, pulp and paper manufacturing, and industries that produce phenol resins. According to the United States Environmental Protection Agency (US EPA), phenol is classified as priority pollutants, with its concentration in wastewater not exceeding 1 mg/L [2].

These contaminants are commonly discharged from numerous industrial sectors, such as petroleum, petrochemicals, coal conversion, pulp and paper, pesticides, pharmaceuticals, and phenol resin production [3]. In addition to their environmental impact, phenol poses significant health risks. It is toxic and can lead to both acute and chronic health problems, including respiratory issues, muscle weakness, tremors, coma, skin irritation, vertigo, anorexia, and diarrhea [4-5]. Therefore, the removal of phenol from wastewater is crucial for protecting both public health and aquatic ecosystems.

Various treatment methods have been developed for phenol removal, including coagulation, chemical oxidation, solvent extraction, membrane filtration, and

reverse osmosis [6]. However, these methods often come with disadvantages, such as high operational costs, excessive sludge generation, and challenges in waste disposal [5]. Among these, adsorption is considered one of the most promising techniques due to its high efficiency and the absence of harmful by-products [7]. Activated charcoal is widely used for phenol adsorption, but its high cost limits its large-scale application [8]. Therefore, the development of cost-effective and efficient alternative adsorbents is urgently needed.

One such promising material is chitosan, a deacetylated derivative of chitin found in the shells of Crustaceans and fungal cell walls. Chitosan is typically produced from chitin through a deacetylation process, either by using strong alkaline solutions at high temperatures or via enzymatic treatment. It is non-toxic, biocompatible, and well known for its antibacterial properties [9]. Despite these advantages, chitosan's adsorption capacity is relatively low. Its surface area and adsorption efficiency can be significantly enhanced by forming nanocomposites with iron oxide nanoparticles, particularly magnetite (Fe_3O_4) [10]. For example, a Fe_3O_4/chitosan/ZIF-8 nanocomposite has shown phenol adsorption of up to 77.21% within 43.33 min at pH 9.91 [11]. To further improve stability and adsorption performance, these composites are often functionalized with organic molecules [12].

In this study, the chitosan/Fe_3O_4 is modified using a reducing sugar derived from sugarcane bagasse hydrolysis [13]. Bagasse is a widely available agricultural byproduct from sugar mills in Indonesia and can be utilized for bioethanol production. Through hydrolysis, cellulose in bagasse is converted into glucose, which serves as the reducing sugar. This process breaks down lignocellulosic biomass into its sugar monomers, and enzymatic hydrolysis is preferred due to its environmentally friendly nature [14]. In this research, the modification of chitosan/Fe_3O_4 nanocomposite with glucose via the Maillard reaction is explored to enhance its phenol adsorption capacity. The resulting material is also expected to exhibit antibacterial properties.

■ EXPERIMENTAL SECTION

Materials

Shrimp shell waste from white shrimp was collected from West Tanjung Jabung Regency, Jambi. Sugarcane dregs (barley) were sourced from Jambi City. The chemicals used in this study included: distilled water (PT Rofa Laboratorium Center), glacial acetic acid 100% (Merck), *Escherichia coli* ATCC 11775 (ThermoScientific), *Staphylococcus aureus* ATCC 33591 (ThermoScientific), nutrient agar (NA), hydrochloric acid (HCl) 37% (Merck), phenol (Merck), sodium hydroxide (NaOH, Merck), 96% ethanol (Merck), $FeCl_2{\cdot}4H_2O$ (Merck), $FeCl_3{\cdot}6H_2O$ (Merck), sulfuric acid 95–97% (Merck), and parafilm tape (Bemis).

Instrumentation

The instruments used in this research included a complete set of laboratory glassware, oven, blender (Miyako), 100 mesh sieve, hydrothermal autoclave reactor (GEA), reflux apparatus, incubator (Memmert IN55), powder X-ray diffraction (XRD) patterns of the composite was recorded on a powder X-ray diffractometer (MiniFlex600, Rigaku), infrared spectrum was recorded on a Fourier Transform Infrared (FTIR IRSPIRIT QATR-S, Shimadzu), vibrating sample magnetometer (VSM), transmission electron microscope (TEM), while the surface morphology was observed by a scanning electron microscope (Hitachi SU3500). Phenol concentration was analyzed using a UV-vis spectrophotometer (BEL photonics).

Procedure

Synthesis of chitosan

Shrimp shell waste was boiled for 15 min and dried in an oven at 110–120 °C. After drying, it was blended and sieved using a 100-mesh sieve. The synthesis of chitosan involved three main steps: demineralization with 1.5 M HCl, deproteinization with 3.5% NaOH, and deacetylation with 60% NaOH. The resulting chitosan was characterized using XRD, FTIR, SEM and TEM.

Synthesis of chitosan/Fe_3O_4 nanocomposites

Chitosan/Fe_3O_4 nanocomposites were synthesized using coprecipitation followed by a hydrothermal method. A total of 1.99 g of $FeCl_2{\cdot}4H_2O$ and 5.41 g of $FeCl_3{\cdot}6H_2O$ were dissolved in 100 mL of distilled water and mixed with 1 g of chitosan. The mixture was transferred into a Teflon-lined hydrothermal reactor

and heated at 150 °C for 12 h. The resulting precipitate was separated using a magnet, washed several times with ethanol and distilled water, and then dried in an oven at 70 °C for 24 h. The final product was characterized by XRD, FTIR, SEM, TEM, and VSM.

Extraction of glucose

The sugarcane bagasse was washed and sun-dried for 48 h. Glucose was extracted by hydrolysis: 5 g of bagasse was placed in a 100 mL Erlenmeyer flask, then 0.1 M H_2SO_4 was added. The mixture was hydrolyzed at 121 °C for 15 min, filtered, and the glucose content was analyzed.

Modification of chitosan/Fe_3O_4 nanocomposite with glucose

A 1% (w/v) solution of chitosan/Fe_3O_4 nanocomposite was dissolved in 1% (v/v) acetic acid. Then, 1% (w/v) glucose was added and stirred until fully dissolved. The mixture was refluxed at 65 °C for 1–7 days, depending on the observation of color change. The resulting mixture was neutralized to pH 6 using 2 M NaOH, then centrifuged at 8000 rpm for 15 min. The supernatant was dialyzed in distilled water for 4–6 days, and the dialyzed product was dried in an oven at 70 °C. The chitosan/Fe_3O_4/glucose nanocomposite was characterized using FTIR, XRD, SEM, VSM, and TEM. Solubility testing was conducted using glacial acetic acid for both modified and unmodified samples.

Preparation of stock solution and phenol standards

A phenol stock solution (1000 mg/L) was prepared by dissolving 1 g of phenol in distilled water and diluting to 1 L in measuring flask. This stock solution was serially diluted to prepare standard solutions of 25, 50, 75, 100, and 150 mg/L. These solutions were used to evaluate the adsorption capacity of the chitosan/Fe_3O_4 nanocomposite (control) and the glucose-modified nanocomposite. Absorbance was measured at the maximum wavelength using a UV-Vis spectrophotometer, and a calibration curve was constructed.

Phenol adsorption study

Phenol adsorption was studied by varying pH and contact time under constant temperature. A total of 0.05 g of adsorbent was added to 50 mL of 25 mg/L phenol solution and stirred using a horizontal shaker at time intervals of 10, 20, 30, 40, 50, 60, and 70 min. The remaining phenol concentration in solution was measured using a UV-vis spectrophotometer after separating the adsorbent with the magnet.

Antibacterial test

The antibacterial activity was evaluated using the disk diffusion method against *S. aureus* and *E. coli*. Nanocomposite solutions were prepared at concentrations of 0, 12.5, 25, 50, 100, and 200 µg/mL. Each petri dish containing nutrient agar was inoculated with the test bacteria, and 10 µL of each nanocomposite concentration was applied onto 6 mm sterile paper disks. The disks were placed on the agar surface, sealed with parafilm, and incubated at 37 °C for 24 h.

■ RESULTS AND DISCUSSION

The synthesis of chitosan from shrimp shell waste involved several stages, including deproteinization, demineralization, decolorization, and deacetylation. The shrimp shell waste was initially prepared by boiling, drying, and separating it from the shrimp meat. Before undergoing chemical treatment, the dried shells were ground to 80-mesh size. The shrimp shell waste and the resulting chitosan are shown in Fig. 1. Deproteinization was carried out by adding 3.5% NaOH solution to the shrimp shells to break protein bonds. The resulting material was then treated with HCl in the demineralization step to remove minerals bound to the chitin. The release of CO_2 gas indicated the reaction between hydrochloric acid and mineral salts in the shrimp shells [15]. Decolorization using sodium hypochlorite was then performed to remove pigments such as astaxanthin, responsible for the reddish-orange color of

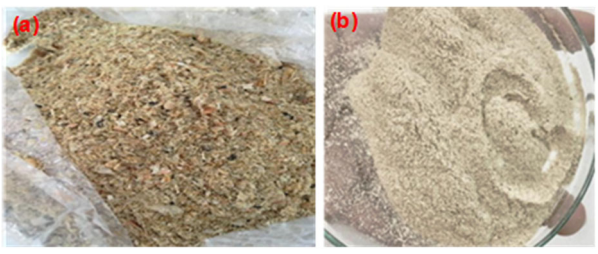

Fig 1. (a) Shrimp shell waste and (b) chitosan synthesis results

of shrimp shells [16]. Untreated chitin appeared brownish, while after treatment it became significantly whiter. Finally, deacetylation was conducted using 60% NaOH to convert acetyl groups into amine groups, yielding chitosan. From 50 g of shrimp shells, 28 g of chitosan were obtained, resulting in a yield of 56%.

Characterization of Synthesized Materials

The nanocomposite was synthesized using the hydrothermal method, with chitosan as the precursor and Fe_3O_4 synthesized via coprecipitation from $FeCl_2{\cdot}2H_2O$ and $FeCl_3{\cdot}6H_2O$ using NaOH as the precipitating agent. Successful synthesis of Fe_3O_4 was confirmed by its magnetic response, as shown in Fig. 2. A 1:1 mass ratio of chitosan to Fe_3O_4 was used for nanocomposite synthesis. The resulting chitosan/Fe_3O_4 powder is shown in Fig. 2. The chitosan/Fe_3O_4/glucose nanocomposite had a black to brownish-black appearance, and a weaker magnetic response than pure Fe_3O_4 due to the non-magnetic nature of chitosan [17].

Bagasse was pretreated by washing, soaking and sun-drying for 48 h, and cutting into fine fibers. Delignification using NaOH and ammonia (1:1) removed 11.57% of lignin. Lignin is dissolved in NaOH and ammonia. Lignin is bound to the NaOH and ammonia solution so that salt is formed, and then the salt dissolves in water during the washing process [18]. The delignification process was carried out on nanocomposite was 7.00 g and after delignification process, it decreased to 6.19 g. This corresponds to an approximate weight loss of 11.58% due to delignification treatment. Hydrolysis was performed on 5 g of sugarcane bagasse using 50 mL of 0.1 M H_2SO_4 at 121 °C for 15 min. the solution was filtered, and glucose content was measured. Hydrolysis of glucose from bagasse resulted in a product yield of 84.6% with a total glucose content of 1.1%.

Modification of chitosan/Fe_3O_4 nanocomposite with glucose (1:1 ratio) in acetic acid resulted in a brownish-black gel (Fig. 2). The solubility test on chitosan/Fe_3O_4/glucose nanocomposite was observed by dissolving the nanocomposite in glacial acetic acid. The first experiment was carried out by adding 10 mL of glacial acetic acid, and chitosan was dissolved, but there were still lumps of nanocomposite powder. Then when

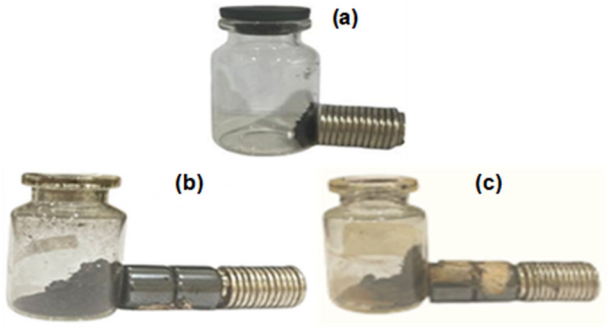

Fig 2. Synthesis of (a) Fe_3O_4 powder, (b) chitosan/Fe_3O_4 nanocomposites, and (c) chitosan/Fe_3O_4/glucose nanocomposites

10 mL of glacial acetic acid was added, the nanocomposite dissolved completely, and there were no lumps. A solubility test in glacial acetic acid showed improved dissolution at higher volumes, indicating better quality chitosan [19].

Structural and Functional Group Characterization

All of the synthesized materials are then characterized using XRD, FTIR, VSM, SEM, and TEM to examine their composition and morphology. The synthesized materials were characterized by using XRD to analyze chitosan that has been modified with glucose by observing the diffraction peaks. In Fig. 3, XRD patterns graph, a peak with increasing intensity was found at an angle (2θ) of 30–40°. In chitosan, which has been modified with Fe_3O_4 and glucose, several peaks are different from those in chitosan. The differences in the peaks produced indicate that Fe_3O_4 and bagasse have been distributed in chitosan.

The XRD patterns of chitosan show that chitosan has a characteristic diffraction peak at 19.6°. Based on the characterization data, this angle is also owned by chitosan/Fe_3O_4 nanocomposites and chitosan/Fe_3O_4/glucose nanocomposites which have the same peak. Based on JCPDS standard data for Fe_3O_4 No. 00-019-0629 has an angle of 2θ with 6 characteristic peaks, namely at 30.05°, 35.42°, 43.05°, 53.40°, 56.94° and 62.52° [20]. The diffractogram results in Fig. 3(b) show that chitosan/Fe_3O_4 nanocomposite has been successfully synthesized. The diffractogram results in Fig. 3(c) show that the chitosan/Fe_3O_4/glucose nanocomposite has been successfully synthesized, which can be proven by

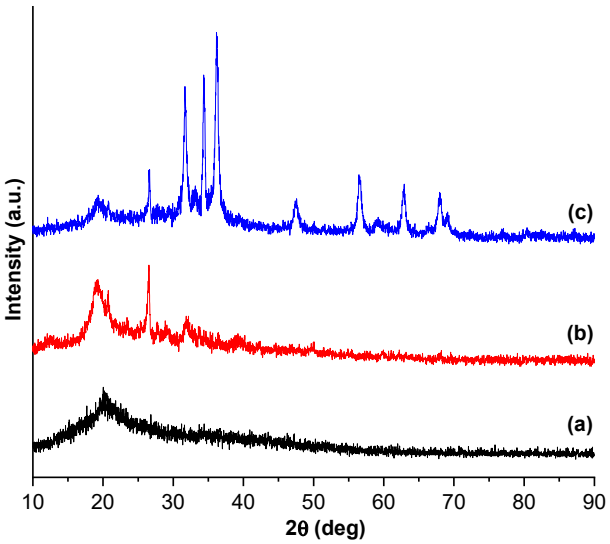

Fig 3. XRD results of (a) chitosan, (b) chitosan/Fe_3O_4 nanocomposite, and (c) chitosan/Fe_3O_4/glucose nanocomposite

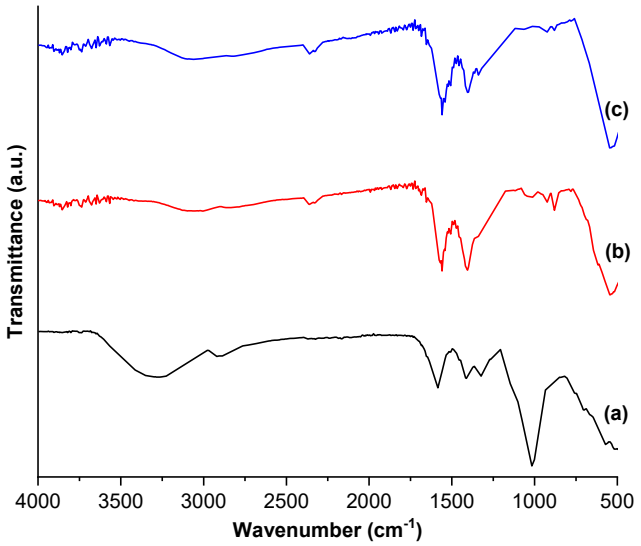

Fig 4. FTIR spectra of (a) chitosan, (b) chitosan/Fe_3O_4 nanocomposite, and (c) chitosan/Fe_3O_4/glucose nanocomposite

the standard data of JCPDS No. 00-021-1272 which has an angle of 2θ with 6 characteristic peaks, namely at 24.8°, 37.3°, 47.6°, 53.5°, 55.1°, and 62.2°. There were some significant differences between Fig. 3(b) and 3(c), where Fig. 3(c) shows more peaks including 53.5°, 55.1°, 62.2°, 67.97°, and 69.08°. When compared between chitosan/Fe_3O_4 nanocomposite and chitosan/Fe_3O_4/glucose nanocomposite, many new angles were formed in the chitosan/Fe_3O_4/glucose nanocomposite. So, it can be concluded that chitosan/Fe_3O_4/glucose nanocomposite was successfully made because there are angles that support each characteristic of glucose [21]. The crystal size of the chitosan/Fe_3O_4/glucose nanocomposite was calculated using the Scherer formula at the highest peak angle of 2θ. Based on the calculation results, the particle size of the chitosan/Fe_3O_4/glucose nanocomposite was 17.21 nm.

The FTIR analysis was utilized to analyze the chitosan obtained from shrimp shell waste, chitosan/Fe_3O_4 nanocomposites, and chitosan/Fe_3O_4/glucose nanocomposites, allowing for the identification of their specific functional groups. In Fig. 4, it can be seen that there is a slight change in the IR spectrum that is not too significant. There is a typical absorption band in chitosan at wave number 3277 cm^{-1}, which indicates the presence of O–H stretching that overlaps with the N–H group. This is marked by the presence of a wide and sharp absorption band. The area of 2895 indicates the presence of aliphatic C–H stretching. Absorption at wave number 1590 indicates the C=O stretching bond of the acetamide group found in the main chain of chitosan. Absorption at 1400 suggests the presence of a C–N bond, while in the area of 1019 is the C–O stretching group. O–H, N–H, C=O, and C–O are typical functional groups of chitosan [22].

Chitosan/Fe_3O_4 nanocomposites and chitosan/Fe_3O_4/glucose nanocomposites show spectrum characteristics that are almost the same as chitosan, but there are some shifts. In addition, new peaks at 531 and 544 cm^{-1} appeared, which were relatively sharper, indicating the interaction between chitosan and Fe_3O_4 through the nitrogen atom in NH_2. The shift to the lower wave set in C=O stretching of chitosan when magnetite and glucose corporate into the framework happened due to bond formation as a result of the composite being synthesized. The data of characteristic peaks in chitosan, chitosan/Fe_3O_4 nanocomposites and chitosan/Fe_3O_4/glucose nanocomposites are attached in Table 1.

The characterization using VSM is performed as well to examine and determine the magnitude of magnetic properties caused by changes in the external magnetic field of Fe_3O_4 as magnetite nanoparticles, changes in the

Table 1. Interpretation data of functional groups from FTIR spectra on chitosan, chitosan/Fe_3O_4 nanocomposites, and chitosan/Fe_3O_4/glucose nanocomposites

Wavenumber (cm^{-1})				Functional groups
Chitosan	Chitosan-Fe_3O_4	Chitosan-Fe_3O_4-glucose nanocomposite	Wavelength range	
3277	3243	3207	3500–3100	–NH
			3600–3200	–OH
2895	2940	2933	2970–2850	–CH (CH_2)
1591	1557	1562	1700–1550	C=O ($NHCOCH_2$–)
1400	1404	1402	1600–1350	C–N
1019	1019	1021	1300–900	C–O (C–O–C)
-	531	544	800–400	Fe–O

magnetic field in chitosan/Fe_3O_4 nanocomposites, and changes in the magnetic field in chitosan/Fe_3O_4/glucose nanocomposites. The resulting curve of the analysis is shown in Fig. 5. The hysteresis curve shows the relationship between magnetization (M) and the external magnetic field (H). The highest saturation magnetization value is in Fe_3O_4, with a value of 78.56 emu/g. The results obtained experienced changes to the saturation moment of pure Fe_3O_4 with a value of 92 emu/g. The saturation value can be impacted by the occurrence of impurities in magnetic particles. In chitosan/Fe_3O_4 nanocomposites and chitosan/Fe_3O_4/glucose nanocomposites, there was a decrease in the saturation moment due to the addition of non-magnetic chitosan and glucose. Particle arrangement density can also influence the reduction in saturation magnetization, making it easy to interact with particles that produce magnetic moments. The denser the particles are in the composition of a particle, the greater the number of magnetic moments, and the amount of magnetic energy will also increase so that its magnetic properties will also increase [23]. The VSM saturation value of chitosan/Fe_3O_4/glucose nanocomposites is 63.4 emu/g, which means that it is superparamagnetic, which is good so that it can be applied as an attractor particle to separate compounds.

Morphological Analysis

Characterization using SEM was performed to determine the surface morphology of the resulting nanocomposite. The SEM result of chitosan in Fig. 6(a)

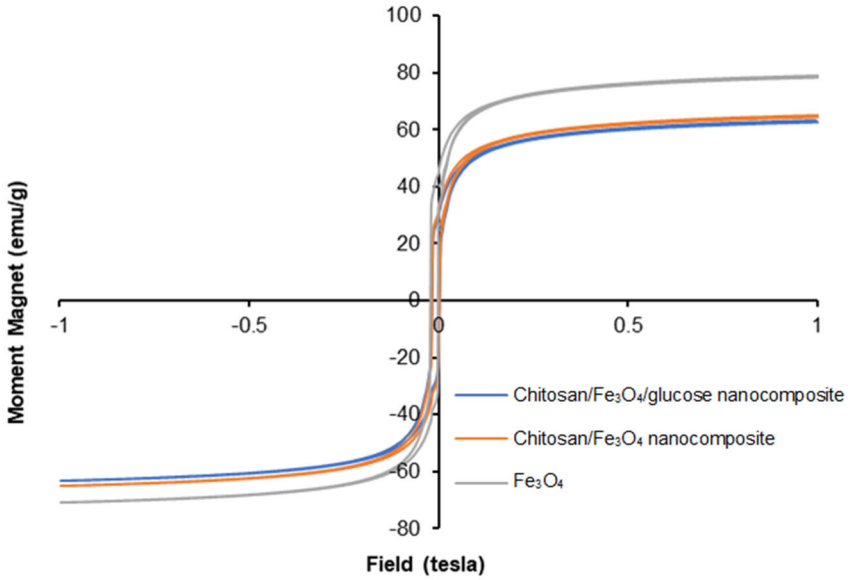

Fig 5. Hysteresis curves of Fe_3O_4, chitosan/Fe_3O_4 nanocomposites, and chitosan/Fe_3O_4/glucose nanocomposites

shows the surface of chitosan that has a non-smooth structure with few granules, while Fig. 6(b) shows the surface of the chitosan/Fe_3O_4/glucose nanocomposite that has many granules with a lighter color. The difference in morphological structure shows the difference between pure chitosan and chitosan that has been added with Fe_3O_4 and glucose. Fe_3O_4 and glucose become a coating and stick to the outside of the chitosan. The chitosan/Fe_3O_4/glucose nanocomposite is in the form of lumps, indicating agglomeration between particles. This is because each particle in chitosan/Fe_3O_4/glucose has strong magnetic properties so they tend to approach each other [24].

Chitosan/Fe_3O_4/glucose nanocomposites were also characterized using TEM. The purpose of characterization using TEM is to see the morphological characteristics of chitosan/Fe_3O_4/glucose nanocomposites by looking at the crystal structure, determining particle size, and analyzing the microstructure. Based on Fig. 7, the results of the chitosan/Fe_3O_4/glucose nanocomposite morphology or internal structure are obtained. The chitosan/Fe_3O_4/glucose nanocomposite has a unified and stacked structure known as aggregation. TEM photos show a distribution pattern. In the image, there are dark and bright centers. Darker points spread to the brighter parts. In this image, an aggregate phase is visible with a darker black color intensity at several points, indicating the aggregation of Fe_3O_4 particles. According to the results of previous studies on Fe_3O_4 agglomeration, there is a quite large agglomeration, and particles tend to form clusters [25]. Based on the results of diameter measurements at several particle points, the particle size of the chitosan/Fe_3O_4/glucose nanocomposite shows the size of nanoparticles with an average measurement of 7.3 nm.

Phenol Adsorption Study

Determination of the optimum condition based on the pH solution is determined in phenol pH ranging from 2–7. Based on Fig. 8, the optimum pH condition of phenol is 4 with an adsorption percentage of 27.67%. The higher the concentration of H^+ ions, the greater the protonation of the adsorbent active group with the presence of OH for chitosan, from NH_2^+ to NH_3^+. This leads the adsorption of phenol to decrease because no more free electron pairs can

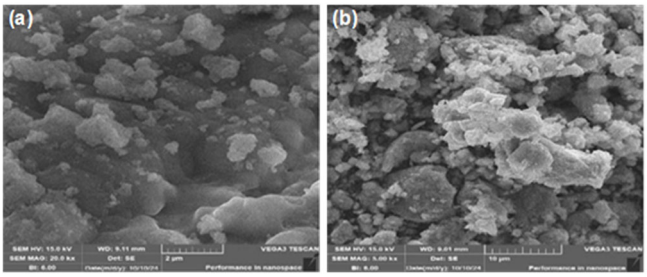

Fig 6. SEM morphology of (a) chitosan and (b) chitosan/Fe_3O_4/glucose nanocomposite

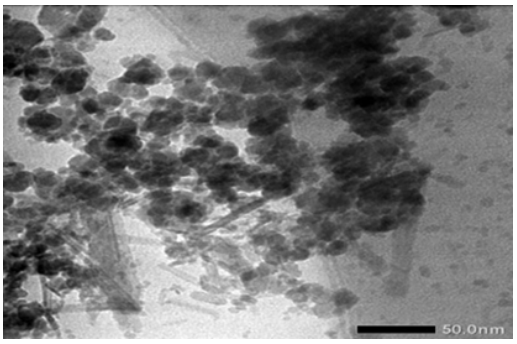

Fig 7. TEM characterization results of chitosan/Fe_3O_4/glucose nanocomposites

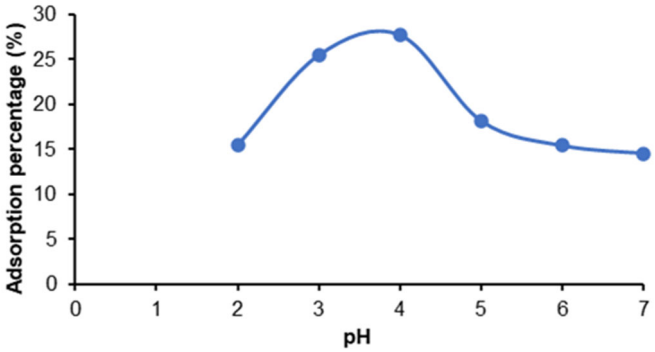

Fig 8. The effect of pH on adsorption of chitosan and chitosan/Fe_3O_4/glucose nanocomposites on phenol

bind. Meanwhile, at pH 4, phenol is thought to have a higher affinity to bind to the adsorbent active group, so there is an increase in the amount of phenol adsorbed. Then the amount of phenol adsorbed decreases with increasing pH.

The effect of phenol adsorption time by chitosan/Fe_3O_4/glucose nanocomposite aims to find the optimum time in the phenol adsorption process. The effect of time is an important factor in the adsorption process to see the collision interaction between the adsorbent and adsorbate. The time used for the

adsorption process was varied, i.e., 20, 30, 40, 50, 60, and 70 min. The concentration of residual phenol was calculated using a UV-vis spectrophotometer with a wavelength of 760 nm. The following curve of the effect of time on the amount of phenol being adsorbed is presented in Fig. 9. The chitosan/Fe_3O_4/glucose nanocomposite absorbs more phenol than chitosan. The longer the adsorption contact time on phenol, the higher the adsorption concentration. In the chitosan/Fe_3O_4/glucose nanocomposite, there is an increase and decrease in the adsorption concentration due to the influence of the phenol that is adsorbed at that time, which is not yet stable. The optimum time for phenol absorption on chitosan and chitosan/Fe_3O_4/glucose nanocomposite is 60 min. Chitosan and chitosan/Fe_3O_4/glucose nanocomposite at that minute have reached equilibrium, with adsorption percentages of 7.18 and 16.46%, respectively. At optimum conditions, the surface of the adsorbent will be filled with phenol so that it cannot absorb the adsorbate because the surface of the adsorbent is fully occupied [26].

Antibacterial Activity

The antibacterial activity of the synthesized chitosan/Fe_3O_4/glucose nanocomposite was evaluated against *E. coli* and *S. aureus* using the disk diffusion method. The results showed that the diameter of the inhibition zones varied depending on the concentration of the nanocomposite. Higher concentrations led to larger inhibition zones, suggesting stronger antibacterial activity [27].

As shown in Fig. 10, the type of bacteria significantly influenced the inhibition zone size. The nanocomposite exhibited greater antibacterial efficacy against *E. coli* compared to *S. aureus*. This can be attributed to differences in bacterial cell wall structure. The nanocomposite adheres to the bacterial cell wall, penetrates the membrane, and disrupts cellular function, leading to cytoplasmic leakage and bacterial death [28]. In addition to its phenol adsorption capability, the chitosan/Fe_3O_4/glucose nanocomposites demonstrate promising antibacterial properties, making it a multifunctional material for wastewater treatment.

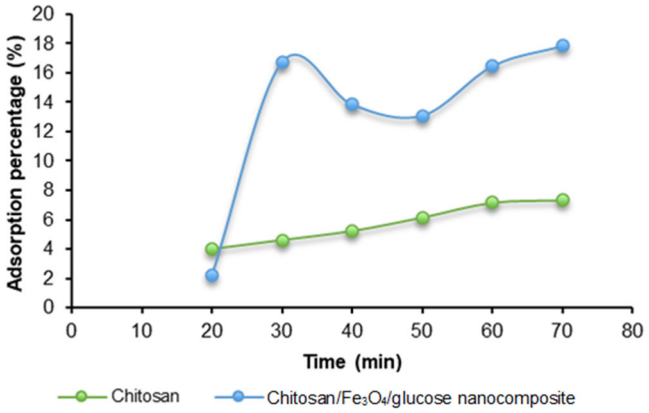

Fig 9. The effect of contact time on adsorption of chitosan and chitosan/Fe_3O_4/glucose nanocomposites

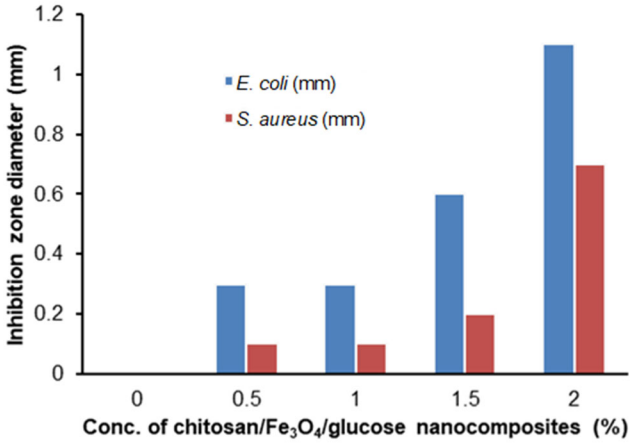

Fig 10. Diameter of the inhibition zone of chitosan/Fe_3O_4/glucose nanocomposite in *E. coli* and *S. aureus*

■ CONCLUSION

This study demonstrated the successful of a chitosan/Fe_3O_4/glucose nanocomposite with phenol adsorption capacity of 16.46% at 60 min and antibacterial activity against *S. aureus* and *E. coli*. For greater reproducibility and optimization, further studies involving pH and temperature variation are recommended.

■ ACKNOWLEDGMENTS

The authors would like to acknowledge the support of *Kementerian Pendidikan, Kebudayaan, Riset dan Teknologi Republik Indonesia* for providing research *Hibah Penelitian Dosen Pemula* 2024 with contract number 002/PLT/LPPM/2024.

■ CONFLICT OF INTEREST

There is no conflict of interest to be declared.

■ AUTHOR CONTRIBUTIONS

Widya Twiny Rizki conceived and designed the experiments provided essential reagents and materials, contributed to data analysis, performed the experimental work, and drafted the manuscript. Siti Marwah Lestari conducted the experiments and was responsible for data analysis and interpretation. Vindi Annisa Rahmah participated in the experimental work and contributed to manuscript preparation. Rd Rahmat Dauli participated in the throughtout making and edited graphic datas. All authors reviewed and agreed to the final version of this manuscript.

■ REFERENCES

[1] Tadić, V., Petrić, M., Uzelac, B., Milošević, S., Vujčić, Z., Stevanović, J., and Tadić, J., 2018, Phenol removal from solution using different varieties of lettuce (*Lactuca sativa* L.) – Part 1, *Sci. Hortic.*, 231, 210–218.

[2] Raza, W., Lee, J., Raza, N., Luo, Y., Kim, K.H., and Yang, J., 2019, Removal of phenolic compounds from industrial wastewater based on membrane-based technologies, *J. Ind. Eng. Chem.*, 71 (1), 1–18.

[3] Albedah, M.A., Hamoudi, M.R., Sadon, S.H., Oussama, E., and Le, Q.H., 2023, Study of phenol removal from wastewater petroleum industry using molecular dynamics method for two-dimensional adsorbent from the aqueous environment, *Eng. Anal. Boundary Elem.*, 147, 69–75.

[4] Erattemparambil, K., Mohan, L., Gnanasundaram, N., and Krishnamoorthy, R., 2023, Insights into adsorption theory of phenol removal using a circulating fluidized bed system, *Arabian J. Chem.*, 16 (6), 104750.

[5] Basuki, T.M., Indrawati, D.R., Nugroho, H.Y.S.H., Pramono, I.B., Setiawan, O., Nugroho, N.P., Nada, F.M.H., Nandini, R., Savitri, E., Adi, R.N., Purwanto, P., and Sartohadi, J., 2024, Water pollution of some major rivers in Indonesia: The status, institution, regulation, and recommendation for its mitigation, *Pol. J. Environ. Stud.*, 33 (4), 3515–3530.

[6] Grace Pavithra, K., Sundar Rajan, P., Arun, J., Brindhadevi, K., Hoang Le, Q., and Pugazhendhi, A., 2023, Review on recent advancements in extraction, removal, and recovery of phenol from phenolic wastewater: Challenges and future outlook, *Environ. Res.*, 237, 117005.

[7] Afsharnia, M., Saeidi, M., Zarei, A., Narooie, M.R., and Biglari, H., 2016, Phenol removal from aqueous environment by adsorption onto pomegranate peel carbon, *Electron. Physician*, 8 (11), 3248–3256.

[8] Yu, L., Gamliel, D.P., Markunas, B., and Valla, J.A., 2021, A promising solution for food waste: Preparing active carbons for phenol removal from water streams, *ACS Omega*, 6 (13), 8870–8883.

[9] Hameed, A.Z., Raj, S.A., Kandasamy, J., Baghdadi, M.A., and Shahzad, M.A., 2022, Chitosan: A sustainable material for multifarious applications, *Polymers*, 14 (12), 2335.

[10] Sharifi, M.J., Nouralishahi, A., Hallajisani, A., and Askari, M., 2021, Magnetic chitosan nanocomposites as adsorbents in industrial wastewater treatment: A brief review, *Cellul. Chem. Technol.*, 55 (2), 185–205.

[11] Keshvardoostchokami, M., Majidi, M., Zamani, A., and Liu, B., 2021, Adsorption of phenol on environmentally friendly Fe_3O_4/chitosan/zeolitic imidazolate framework-8 nanocomposite: Optimization by experimental design methodology, *J. Mol. Liq.*, 323, 15064.

[12] Francis, A.O., Zaini, M.A.A., Muhammad, I.M., Abdulsalam, S., and El-Nafaty, U.A., 2023, Physicochemical modification of chitosan adsorbent: A perspective, *Biomass Convers. Biorefin.*, 13 (7), 5557–5575.

[13] Saroj, P., Manasa, P., and Narasimhulu, K., 2024, Enhanced reducing sugar production by blending hydrolytic enzymes from *Aspergillus fumigatus* to improve sugarcane bagasse hydrolysis, *Environ. Sci. Pollut. Res.*, 31 (35), 48085–48102.

[14] Amândio, M.S.T., Rocha, J.M.S., and Xavier, A.M.R.B., 2023, Enzymatic hydrolysis strategies for cellulosic sugars production to obtain bioethanol from *Eucalyptus globulus* bark, *Fermentation*, 9 (3), 241.

[15] Pohling, J., Dave, D., Liu, Y., and Murphy, W., 2022, Two-step demineralization of shrimp (*Pandalus borealis*) shells using citric acid: An environmentally friendly, safe and cost-effective alternative to the traditional approach, *Green Chem.*, 24 (3), 1141–1151.

[16] Aridi, A.S., Yusof, Y.A., Chin, N.L., Ishak, N.A., Yusof, N.A., and Manaf, Y.N., 2021, Physicochemical properties of chitosan extracted from *Leucaena leucocephala* pods using deprotenization and decolorization steps, *IOP Conf. Ser.: Earth Environ. Sci.*, 709 (1), 012038.

[17] Mukhayani, F., Kamiya, Y., Otomo, R., Kunarti, E.S., and Nuryono, N., 2024, Modification of chitosan-coated magnetic material with glycidyltrimethylammonium chloride and its application as heterogeneous base catalyst for levulinic acid esterification, *Mater. Adv.*, 5 (9), 3838–3849.

[18] Ameram, N., Muhammad, S., Nik Yusof, N.A.A., Ishak, S., Ali, A., Shoparwe, N.F., and Ter, T.P., 2019, Chemical composition in sugarcane bagasse: Delignification with sodium hydroxide, *Malays. J. Fundam. Appl. Sci.*, 15 (2), 232–236.

[19] Santoso, J., Adiputra, K.C., Soedirga, L.C., and Tarman, K., 2020, Effect of acetic acid hydrolysis on the characteristics of water soluble chitosan, *IOP Conf. Ser.: Earth Environ. Sci.*, 414, 012021.

[20] Alfredo Reyes Villegas, V., Isaías De León Ramírez, J., Hernandez Guevara, E., Perez Sicairos, S., Angelica Hurtado Ayala, L., and Landeros Sanchez, B., 2020, Synthesis and characterization of magnetite nanoparticles for photocatalysis of nitrobenzene, *J. Saudi Chem. Soc.*, 24 (2), 223–235.

[21] Pietrzyk, P., Phuong, N.T., Olusegun, S.J., Hong Nam, N., Thanh, D.T.M., Giersig, M., Krysiński, P., and Osial, M., 2022, Titan yellow and Congo red removal with superparamagnetic iron-oxide based nanoparticles doped with zinc, *Magnetochemistry*, 8 (8), 91.

[22] Ayodele, O., Okoronkwo, A.E., Oluwasina, O.O., and Abe, T.O., 2018, Utilization of blue crab shells for the synthesis of chitosan nanoparticles and their characterization, *Songklanakarin J. Sci. Technol.*, 40 (5), 1043–1047.

[23] Asgari, E., Sheikhmohammadi, A., and Yeganeh, J., 2020, Application of the Fe_3O_4-chitosan nano-adsorbent for the adsorption of metronidazole from wastewater: Optimization, kinetic, thermodynamic and equilibrium studies, *Int. J. Biol. Macromol.*, 164, 694–706.

[24] Covaliu, C.I., Matei, E., Stoian, O., and Paraschiv, G., 2020, Magnetic nanocomposite material containing chitosan polymer used in wastewater depollution processes, *Mater. Plast.*, 57 (4), 70–76.

[25] Wang, F., Liu, J., Wang, X., Kong, J., and Qiu, S., 2012, Synthesis of hollow Fe_3O_4 at ZnO at anatase TiO_2 core-shell structured spheres, *Ceram. Int.*, 38 (8), 6899–6902.

[26] Darjito, D., Purwonugroho, D., and Ningsih, R., 2014, The adsorption of Cr(IV) ions using chitosan-alumina adsorbent, *J. Pure Appl. Chem. Res.*, 3 (2), 53–61.

[27] Prayoga, A., Hasibuan, P.A.Z., and Yuandani, Y., 2021, Antibacterial activity of patch silver nanoparticles and chitosan with cellulose nanofibers carriers against *Staphylococcus aureus* and *Escherichia coli*, *Indones. J. Pharm. Clin. Res.*, 4 (2), 15–21.

[28] Pascual, A.M.D, 2020, Antibacterial action of nanoparticle loaded nanocomposites based on graphene and its derivatives: A mini-review, *Int. J. Mol. Sci.*, 21 (10), 3563.